ACS OMEGA

http://pubs.acs.org/journal/acsodf

Article

Effect on Human Vascular Endothelial Cells of Au Nanoparticles Synthesized from *Vitex mollis*

Abraham Arizmendi-Grijalva, Aarón Alberto Martínez-Higuera, Jesús Adriana Soto-Guzmán, Juan Manuel Martínez-Soto, Ericka Rodríguez-León, César Rodríguez-Beas, Luis Fernando López-Soto, Francisco Javier Alvarez-Cirerol, Nadia Garcia-Flores, Pedro Cortés-Reynosa, Eduardo Pérez-Salazar, and Ramón Iñiguez-Palomares*

Cite This: *ACS Omega* 2021, 6, 24338−24350

Read Online

ACCESS | Metrics & More | Article Recommendations | Supporting Information

ABSTRACT: A green method for synthesizing gold nanoparticles is proposed using hydroethanolic extract of *Vitex mollis* fruit (Vm extract) as a reducer and stabilizer. The formation of gold nanoparticles synthesized with Vm extract (AuVmNPs) was monitored by measuring the ultraviolet−visible spectra. The morphology and crystalline phase were determined using scanning electron microscopy, X-ray diffraction, and high-resolution transmission electron microscopy. Synthesized nanoparticles were generally spherical, and the size distribution obtained by transmission electron microscopy shows two populations with mean sizes of 12.5 and 22.5 nm. Cell viability assay using MTT and cellular apoptosis studies using annexin V on human umbilical vein endothelial cells (HUVECs) and the human mammary epithelial cell line (MCF10A) indicate that AuVmNPs have low toxicity. Cell migration tests indicate that AuVmNPs significantly inhibit HUVEC cell migration in a dose-dependent manner. The evaluation of the localization of AuVmNPs in HUVECs using confocal laser scanning microscopy indicates that nanoparticles penetrate cells and are found in the cytosol without preferential distribution and without entering the nucleus. The inhibitory effect on cellular migration and low toxicity suggest AuVmNPs as appropriate candidates in future studies of antiangiogenic activity.

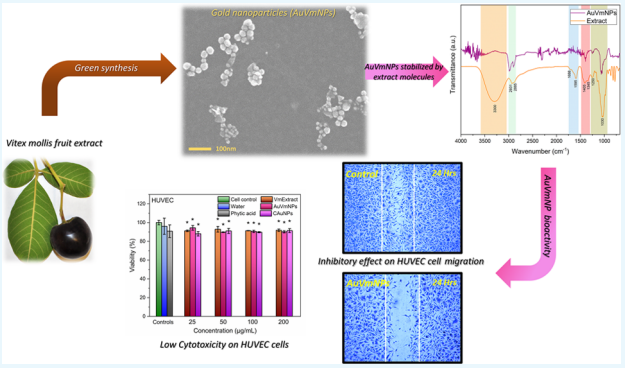

INTRODUCTION

AuNPs have turned out to have physical and biological properties that have been studied over the years, obtaining great medical relevance.[1−8] Generally, the synthesis of nanoparticles is carried out by chemical methods in which toxic reactants are used, the waste being harmful to the environment, in addition to being necessary to eliminate the residues present on the NPs for biological uses. The synthesis of metal NPs using plant extracts has gained importance among the proposals of sustainable chemistry.[9−13] The bioactive compounds of the extracts act as reducing agents in the synthesis reaction and as stabilizers when adsorbed on the surface of the NPs forming a composite with interesting therapeutic properties.[14−16] This aspect has the advantage of being an environmentally friendly method because generally, the synthesis reaction of NPs is carried out at room temperature without requiring an energy contribution in the process and is carried out in a single step because it does not require additional molecules to stabilize the system since the same reducing molecules in the extract act as a stabilizer for the NPs formed.[17]

Angiogenesis is the formation of new blood vessels from pre-existing ones and is known as one of the distinctive marks associated with cancerous processes.[18] In grown organisms, the proliferation of blood vessels is important for the growth and functioning of female reproductive organs, such as the ovaries and endometrium during the menstrual cycle, as well as during pregnancy in the placenta and mammary glands. However, in most of the grown tissues, angiogenesis is highly restricted, and the vessels' growth process occurs only in wounds and fracture regenerations.[19] Although angiogenesis is a physiological process given in embryonic development and wound healing, it can have pathological implications since it is essential in the development of tumors because it provides the tumors with

Received: March 20, 2021
Published: September 16, 2021

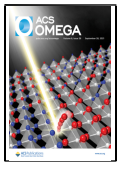

oxygen and nutrients for growth; therefore, there is interest in inhibiting the process without affecting healthy cells.[20,21]

Nanoparticles can play an important role as angiogenesis-inhibiting agents, the effect of which is related to their characteristics such as nanoparticle size and surface charge.[22−28] In particular, gold nanoparticles have shown a remarkable ability to slow down angiogenic processes by suppressing endothelial cell migration.[28−30]

Vitex mollis is a tree located mainly along the west coast of Mexico where its fruit is known as uvalama. Traditionally, the fruit has been consumed for the treatment of diseases such as fever and diarrhea and even used as an anti-inflammatory agent. Chemical constituents from the fruit include fructose, melanins, catechins, anthraquinone, and inositol hexakisphosphate.[31] Melanins are known to be high-molecular-weight molecules that form pigments from the polymerization of phenolic compounds[32] and can be classified into eumelanin (dark brown/black), pheomelanin (yellow/red), and allomelanin, specific to the plant kingdom.[33] They also show great antioxidant capacity, which makes them attractive as reducing agents in nanomaterials synthesis.[34−37]

In this work framed in the "green" chemistry context, we synthesize gold nanoparticles using a hydroethanolic extract from the *Vitex mollis* fruit through a single-step method. The products obtained were characterized by spectroscopic and microstructural techniques. In vitro cytotoxicity tests of these materials were performed on HUVECs and through a scratch test, and the effects on cell migration were evaluated.

EXPERIMENTAL SECTION

The reagents tetrachloroauric acid ($HauCl_4$, 99% purity), 3-(4,5-dimethylthiazol-2-yl)-2,5-diphenyltetrazolium bromide (MTT), 2,2-diphenyl-1-picrylhydrazyl (DPPH), 6-hydroxy-2,5,7,8-tetramethylchroman-2-carboxylic acid (Trolox), Folin−Ciocalteu, dimethyl sulfoxide (DMSO), Dulbecco's modified Eagle medium (DMEM), crystal violet, and mitomycin C were obtained from Sigma Aldrich. Ethanol was acquired from Fermont (99 % purity), and ultrapure water was obtained from a Milli-Q apparatus. All glassware has been properly washed with ultrapure water and ethanol and then dried in an oven before use. All the other used reagents had the highest purity grade.

Extract Preparation. *Vitex mollis* fruits were collected from the Universidad de Sonora central campus in Hermosillo, Sonora in June, and it was ensured that the collected products were of a uniform black color characteristic of ripe fruits. They were washed with three-distilled water to remove dust, subsequently with ultrapure water, and dried in an oven for a week at 45°C. Then, 200 g of the dried fruit was weighed and placed on a one-liter glass container adding a 70/30 (v/v) mixture of ethanol and ultrapure water macerating the fruit for two months. After the maceration time, an 8 μm Whatman paper filter was used to remove the solid part of the extract; subsequently, a 0.2 μm acrodisc filter was used, and the filtration was vacuum-assisted in a Kitasato flask. The already filtered extract was placed in a 2/210 Buchi rotary evaporator to remove ethanol from the solution. Finally, the extract was frozen at −80 °C and placed in a lyophilizer LABCONCO FreeZone 1L to remove the water and obtain a solid product from the extract.

Green Synthesis of AuVmNPs. For AuVmNP production, 0.5 g of extract was weighed and dissolved at 50 mL of an ethanol and water mixture (1:1), applying vigorous shaking on a vortex mixer (Fisher Scientific) at 3000 rpm for 5 min. Then, 10 mL of this extract solution, 85 mL of ultrapure water, and 5 mL of 0.01 M $HAuCl_4$ aqueous solution were placed in a glass container. The mixture was placed in the presence of sunlight for 1 h under magnetic agitation at 1000 rpm. Once the AuVmNPs were synthesized, they were centrifuged at 14000 rpm for 1 h, the supernatant was removed, and the precipitate was resuspended in ultrapure water by sonication. The procedure was repeated twice, and the last centrifugation was performed by resuspending nanoparticles in ethanol and then centrifuging at 14000 rpm. The supernatant was removed, and the precipitated nanoparticles were dried in an oven at 45 °C for 2 h. The recovered nanoparticle powders were deposited in glass culture tubes with a screw cap (O.D. × L 13 × 100 mm). These particles were weighed and added to the appropriate solvent volume (ultrapure water) to obtain a nanoparticle concentration of 2 mg/mL. To ensure complete redispersion of the nanomaterials, the glass tubes were sonicated for 2 h in an ultrasonic cleaner at 40 kHz (Branson 2510).

Gold nanoparticles used as a control were synthesized by the chemical reduction method proposed by Turkevich.[38] For it, 150 mL of $HAuCl_4$ (1 mM) was warmed in a plate with magnetic stirring, until it reached boiling, the stirring was kept for 3 min, and then, 15 mL of a sodium citrate solution (78 mM) was added. Immediately after adding sodium citrate, the solution in the beaker lost its color and to time transcurrent acquired an intense purple color after 10 min. A small volume of the sample was required to obtain an absorption spectrum of the nanomaterial this time. It was continuously stirred for 5 min, and no changes were detected in the colloidal nanoparticles' dispersion color. The final product of gold nanoparticles (CAuNPs) was allowed to cool to room temperature and characterized by UV−vis spectroscopy, DLS, zeta potential, and SEM.

Characterization Techniques. *UV−Visible Spectroscopy.* The UV−visible spectra were measured at the range of 200 to 900 nm on a PerkinElmer Lambda 45 double-beam spectrometer with a slit of 0.5 nm with a velocity of 480 nm per minute. AuVmNP formation kinetics was determined by measuring the absorbance at 558 nm every 3 min, while the NP synthesis reaction was developed inside the quartz cell under magnetic stirring and sunlight illumination conditions.

Antioxidant Activity by DPPH. The DPPH free radical scavenging activity of the Vm extract, at different concentrations (15.6, 31.25, 62.5, 125, and 250 μg/mL), was measured by using a spectrometric method as briefly described below. A DPPH ethanolic solution (300 μM) was prepared, and then, equal volumes (100 μL) of this solution and extract samples were mixed and kept in darkness at room temperature for 2 h. Later, absorbance was registered at 517 nm. Results were expressed as a percentage decrease concerning control values. The percentage of scavenging activity was computed with eq 1

$$\%\text{scavenging activity} = \frac{A_{\text{control}} - A_{\text{sample}}}{A_{\text{control}}} \times 100 \quad (1)$$

where A_{control} is the absorbance of the DPPH radical dissolved only on ethanol and A_{sample} corresponds to DPPH in the presence of Vm extract. All the tests were conducted in triplicate, and from the experiment was determined the 50% inhibitory concentration (IC_{50}). Vitamin C at 70 μmol/L was used as an antioxidant standard.

https://doi.org/10.1021/acsomega.1c01506
ACS Omega 2021, 6, 24338−24350

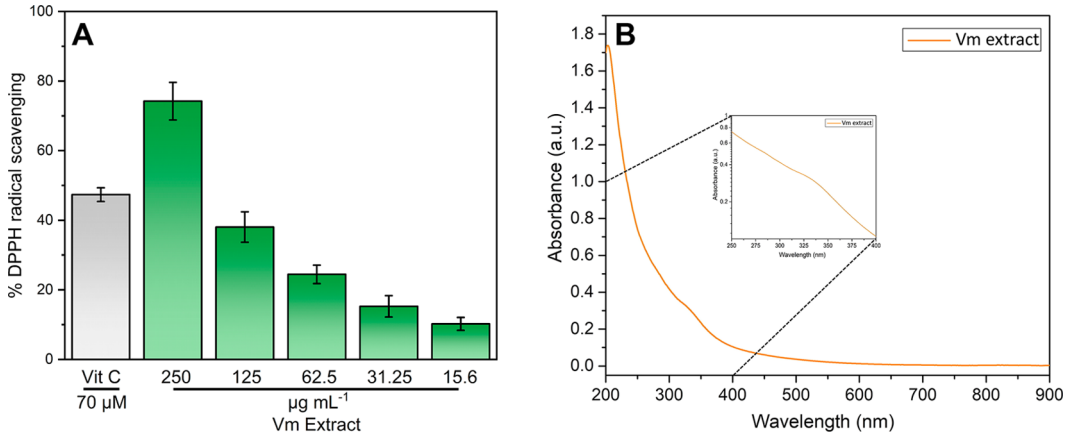

Figure 1. (A) Antioxidant capacity (DPPH) and (B) UV−vis spectrum of *Vitex mollis* extract.

Total polyphenol determination of Vm extract was carried out using the Folin−Ciocalteu reagent with some modifications to the referenced protocol by Jiménez-Estrada et al.[39] Ten microliters of Vm extract at different concentrations was diluted with 80 μL of ultrapure water and further mixed with 60 μL of a 5% sodium carbonate solution and 40 μL of Folin−Ciocalteu (0.25 N) completing a total volume of 280 μL. The sample was left for 1 h, and absorbance was measured at 750 nm. The concentration of total phenolic compounds in Vm extract was expressed in mg of gallic acid equivalent (mg GAE/g) per gram of dry plant.

IR Spectroscopy. An FTIR PerkinElmer Frontier provided with a GladiATR diamond accessory was used. The spectrum was obtained on a transmittance mode and was scanned registering the spectrum with 32 scans at a resolution of 2 cm^{-1}, from 4500 to 500 cm^{-1}.

DLS and Zeta Potential. A Malvern Zetasizer ZS equipment was used to perform measurements of the zeta potential, the Smoluchowski model was used to calculate zeta potential values of nanoparticles in aqueous media, and dynamic light scattering (DLS) was measured at a constant temperature of 25 °C, with a 4 mW laser (633 nm) and a detection angle of 173°. Measurements of the zeta potential and DLS were performed for CAuNPs and AuVmNPs.

Transmission Electron Microscopy. The characterization of sizes and shapes of nanoparticles was carried out by TEM using a Jeol 2010F apparatus operated at 200 keV and with a Gatan CCD camera attached to the equipment. The HRTEM was processed with the software DigitalMicrograph.

Scanning Electron Microscopy. The characterization by scanning electron microscopy was carried out in an SEM Jeol JSM-7800F field emission equipment operated at 30 kV that has a secondary electron detector, transmitted electrons (STEM), and energy-dispersive X-ray spectroscopy (EDX) detectors.

X-ray Diffraction. The crystalline structure characterization of the synthesized NPs was carried out on a Bruker D8 QUEST single crystal diffractometer recorded using Cu K$\alpha\lambda$ = 1.5418 Å radiation at room temperature (300 K). Frames were collected via ω/φ scans and then processed to obtain diffractograms of intensity vs 2θ between 30 and 90°. The HighScore Plus software was used for raw data treatment, and a database associated with the software was implemented for the search-match phase identification analyses.

Cell Assays. *Viability.* The viability test was carried out on a 96-well plate. The well was charged with 90 μL of DMEM with 5% FBS and 5000 cells. After the cells adhered, we added 10 μL of AuVmNPs and CAuNPs. The final concentrations of the treatments were 200, 100, 50, and 25 μg/mL. After 24 h, we added to each well 10 μL of MTT at 12 mM in PBS letting it rest in the incubator for 4 h. After that time, we carefully removed the supernatant, and we added 100 μL of DMSO to dissolve the crystals and read the samples in a microplate ELISA reader at 570 nm. Cell viability was computed using eq 2

$$\%\text{cell viability} = (A_{\text{sample}}/A_{\text{control}}) \times 100\% \quad (2)$$

where A_{sample} is the absorbance of the sample and A_{control} is the absorbance of the blank. Viability was evaluated on human umbilical vein endothelial cells (HUVECs) and human mammary epithelial cell lines (MCF10A). Statistical analysis was carried out using one-way ANOVA (Origin software) where $p < 0.05$ was considered significant.

Annexin V-FITC Apoptosis Assay. HUVECs and MCF10A cells were cultured in DMEM with 10% FBS until confluence, and the cells were serum-starved for 24 h and treated with AuVmNPs, *Vitex mollis* extract, and CAuNPs at 50, 100, and 200 μg/mL for 24 h. Negative apoptotic control of cells without any treatment was performed, and H_2O as a vehicle control was used. As a positive apoptotic control, MCF10A cells were UV-treated for 60 min, and HUVEC cells were 70 °C treated for 60 min. After treatments, the cells were collected and washed once in 1X PBS, then once in annexin V 1X binding buffer (eBioscience, Inc.), and resuspended in 100 μL of binding buffer 1X (1×10^6/mL), and 1 μL of FITC-conjugated Annexin V (Biolegend) was added to the cell suspension and incubated for 10 min in the dark. Cells were washed in 1X binding buffer and resuspended in 200 μL of 1X binding buffer, and 1×10^4 events from the region 3 (R3) were analyzed by flow cytometry using a BD FACS Verse flow cytometer (BD Biosciences), see Figure S1.

Cellular Internalization of AuVmNPs. To study the internalization of AuVmNPs in HUVECs, cells were seeded on glass slides and exposed to the gold nanoparticles at 50 μg/mL. After 24 h of incubation, cellular nucleus staining with DAPI and the actin fibers with an anti-β actin antibody coupled to FITC to delimit the cell border was performed. The analysis was carried out with a confocal microscopy device LSM 800 (Carl Zeiss), equipped with three lasers (405, 488,

https://doi.org/10.1021/acsomega.1c01506
ACS Omega 2021, 6, 24338−24350

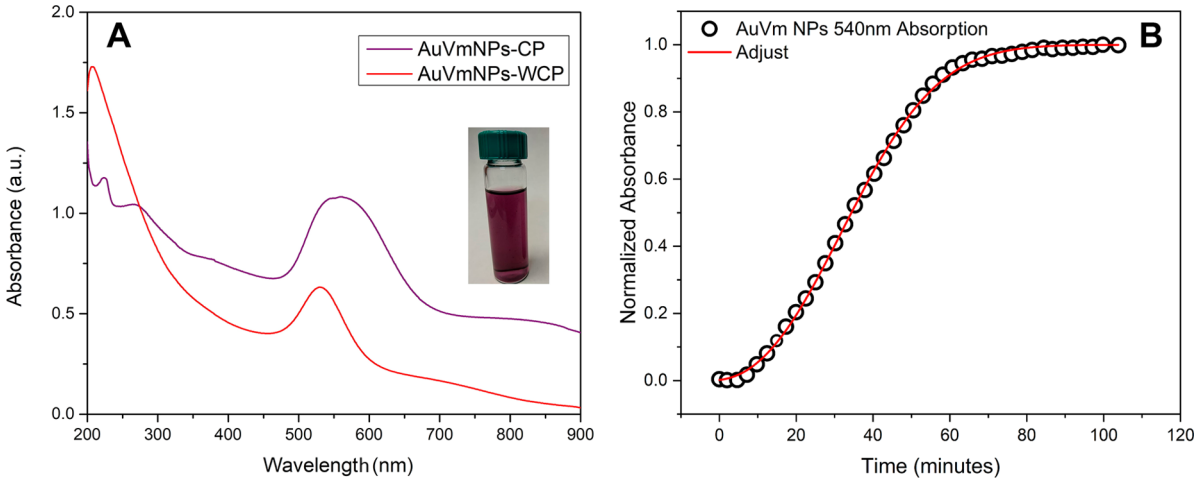

Figure 2. (A) UV−vis spectra of synthesized gold nanoparticles with *Vitex mollis* extract. The original products and those subjected to the cleaning process are exposed. A vial with AuVmNPs is shown in the inset. The figure in (B) corresponds to the kinetics of gold nanoparticle formation. The curve is constructed sensing the intensity of the resonance plasmon at 540 nm over time.

and 640 nm). High-sensitivity GaAsP detectors acquired the fluorescence images, and a photo multiplier tube (PMT) detector collected transmitted laser light through the sample to form bright-field images. DAPI was excited with a 405 nm laser and FITC with a 488 nm laser. Emissions of DAPI and anti-β actin antibodies were collected between 420−480 and 510−600 nm, respectively. To form the AuVmNP images by reflectivity, a 640 nm laser was employed, and the signal was collected between 650 and 700 nm. Blue, green, and red colors were assigned to DAPI, FITCI, and AuVmNPs, respectively.

For 3D cell-AuVmNP reconstruction, a Plan-Apochromatic × 63/1.40 oil objective was used. 3D reconstruction and orthogonal projections were made from 30 images on *Z*-stack mode (total *Z* length = 8 μm), collecting fluorescence signals on separate tracks for each *Z* position.

Scratch Assay. HUVECs were seeded in a 24-well plate at a density of 50,000 cells per well incubated with DMEM with 5% FBS until they reached confluence, and cultures were starved for 12 h using DMEM with 0.1% FBS and treated for 2 h with 12 μM mitomycin C to inhibit proliferation. The scratch test was performed with a yellow pipette tip, and samples were washed two times with sterile PBS and then incubated in DMEM containing 10 vol % AuVmNPs with final concentrations of 200, 100, 50, and 25 μg/mL for 24 h. Wells were also left without NPs as a negative control and as positive control cells treated with 5% FBS; as time passed, the medium was removed, and we added violet crystal solution for 1 min; then, the solution was removed to obtain greater contrast. Cell migration was tracked with an inverted Leica microscope with a 4× objective, and photos were taken with an integrated camera at the beginning and end of the experiment. The images were processed in the software ImageJ, counting by intensity.

RESULTS AND DISCUSSION

Figure 1A shows the antioxidant activity of VM extract. We observe that the behavior of inhibitory activity over the DPPH radical varies proportionally with Vm extract concentration. For 125 μg/mL, inhibitory activity is similar to that of vitamin C (70 μM) employed as a reference. The estimated concentration of 50% inhibition (IC_{50}) is 161.77 μg/mL, which is five times higher than reported for aqueous extracts of fruits of other species of the *Vitex* genus. Total phenolics determination gives a content of 15 ± 0.2 (mg GAE/g). Cuevas-Juárez et al. reported a total phenolics content of 29.48 ± 0.46 (mg GAE/g) for an aqueous extract of *Vitex mollis* fruit obtained at room temperature.[40] This difference can be attributed to the processing of the raw material in the extraction methodologies applied and to the different polarities of the solvents used in each case. Cuevas et al. associated the antioxidant activity of their *Vitex mollis* fruit extract with soluble melanins that are easily extracted using only water with neutral pH,[40] contrary to the standard method of aqueous extraction of melanins in an alkaline medium.[41,42] This property of some melanins to easily solubilize in water can be attributed to their complexation with polar compounds as carbohydrates or proteins, which facilitates their solubility in water.[43]

In Figure 1B, the UV−vis absorption spectrum of the Vm extract is shown from 900 to 200 nm. The behavior closely resembles the UV−vis spectrum of soluble melanin characterized by a linear increase in absorbance from 800 to 600 nm with a subsequent exponential growth at lengths less than 600 nm.[44,45] As a complementary procedure to characterize the melanin presence, the graph log(Abs) versus wavelength is constructed. The behavior associated with these polymers consists of a linear response with a negative slope.[33,41,42] For VM extract, the slope has a value of −0.0046 nm^{-1} (Figure S2), which is very similar to that reported for melanins extracted from *Castanea mollissima*.[46] The inset in Figure 1B corresponds to spectrum magnification on the region from 250 to 400 nm to show the presence of a slight shoulder in 320 nm. Absorption in this region has been reported for melanins from *Vitex mollis* fruit and black tea extracted in an aqueous medium.[40]

In Figure 2A, the absorption spectrum of the gold nanoparticles for the system without the cleaning process (AuVmNPs-WCP) consists of a narrow band corresponding to localized surface plasmon resonance (LSPR) with a maximum at 537 nm. By subjecting the gold nanoparticles to the cleaning process (AuVmNPs-CP), the absorption spectrum shows a broadening of LSPR and the maximum shifts to 550 nm. This bathochromic effect can be explained by the solvent characteristics where the particles are dispersed in each case. Initially,

https://doi.org/10.1021/acsomega.1c01506
ACS Omega 2021, 6, 24338−24350

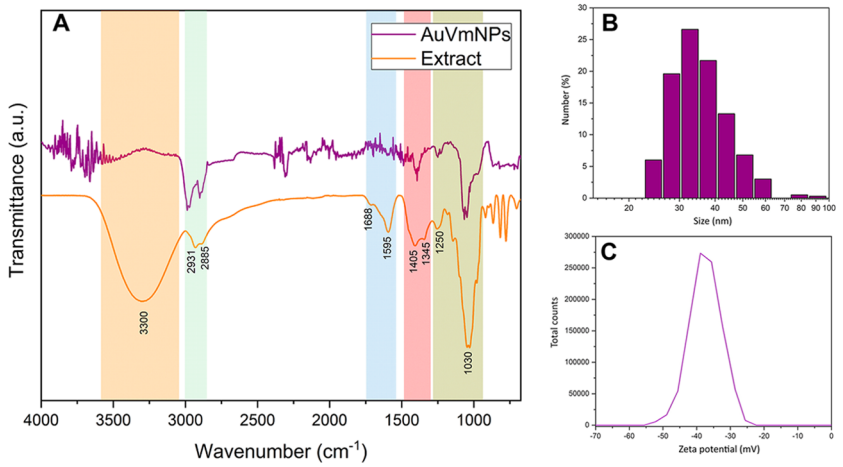

Figure 3. (A) AuVmNPs' and *Vitex mollis* extract's FTIR spectra. (B) AuVmNPs' size distribution by DLS. (C) AuVmNPs' zeta potential.

they were in the aqueous solvent where the synthesis reaction took place, dispersing later in ultrapure water.[47] Interestingly, the AuVmNPs-CP absorption spectrum reveals an absorption band at 275 nm, which can be attributed to phenolic structures coming from VM extract that are responsible for its antioxidant activity. The presence of these compounds even after the cleaning protocol indicates strong complexing with the nanoparticles favoring the stability of the final product. The AuVmNP growth kinetic curve (Figure 2B) was constructed by taking the resonance plasmon absorbance at 540 nm over time and normalizing it concerning the final value of the LSPR absorbance (t = 100 min). For this, the UV−vis spectra were captured at various times while the reaction was carried out for 100 min (see Figure S3). As seen in Figure 2B, the curve has a sigmoidal behavior, and the plateau is reached at 70 min, indicating the end of the reaction. This long synthesis time coincides with other reports of gold nanoparticles obtained with phytoconstituents.[48−50]

Gold nanoparticles produced by the Turkevich chemical method (CAuNPs) are used as controls in the cell viability assays and characterized by various techniques. The UV−vis spectrum of CAuNPs shown in Figure S4 from 400 to 600 nm consists of a well-defined and centered band at 523 nm.

Figure 3A shows the FTIR spectra of Vm extract and AuVmNPs. The −OH stretching vibration produces a broad band with a peak at 3300 cm^{-1} in the Vm extract spectrum. The peaks at 2931 and 2885 cm^{-1}, and the signals at 1405 and 1345 cm^{-1}, correspond respectively to stretching and deformation vibrations of aliphatic C−H. Signals on 1688 and 1595 cm^{-1} are attributed to C═O vibrations of quinone or carboxylic acids and C═C of aromatic rings.[51] The signal located at 1250 cm^{-1} corresponds to phenol C−O−H groups' vibrations, and the intense signal in 1030 cm^{-1} is associated with the C−O−C bonds present in aromatic ethers.[52] In a relevant way, the FTIR spectrum for Vm extract in Figure 3A coincides with great precision with the FTIR spectra reported for soluble melanins obtained from *Vitex mollis* fruit maceration in water.[40] Melanins are dark-colored, high-molecular-weight biopolymers formed by oxidation and polymerization of phenolic compounds.[53] Possible precursors of plant melanin are considered to be catechol or catecholic acids such as caffeic, chlorogenic, protocatechuic, or gallic acids.[54] On the other hand, it is known that melanins in nature form complexes with carbohydrates, proteins, and lipids.[51] Pío-León et al. attributed the solubility of the *Vitex mollis* fruit melanins to the formation of complexes with the abundant carbohydrates on the fruit and reported the presence of IP6 and valeric and benzoic acids.[43]

We suggest that Vm extract phenolic compounds can reduce gold salts for the AuVmNP formation. Several works about metallic nanoparticle synthesis place catecholic acids as excellent reducing agents in a process that involves the oxidation of these compounds to form quinones with the transfer of electrons to the metallic ion.[55−60]

The AuVmNP FTIR spectrum (Figure 3A) indicates that several Vm extract signals are present even after applying a cleaning protocol to remove the extract excess from nanoparticles. We can then establish that extract remanent molecules stabilize AuVmNPs.

The nanoparticle size distribution by DLS and the zeta potential are shown in Figure 3B,C. The AuVmNP average size is 32.7 ± 4.2 nm, and the zeta potential is −40.3 ± 6.6 mV. A high zeta potential absolute value ($|\zeta| \geq 30$) indicates intense repulsive electrostatic interactions between the nanoparticles in solution, preventing aggregation between them, and favors long-term colloidal dispersion stability.[61,62] In Figure S5, CAuNPs show a zeta potential of around −26 ± 4 mV, and the average size determined by DLS is 50 ± 6.6 nm.

The monocrystal XRD pattern of the metal nanoparticles, shown in Figure 4, is recorded between 2θ values 30 and 90° and exhibits crystalline nature. Bragg's diffraction peaks for gold nanoparticles are observed at 38.25, 44.45, 64.85, 77.7, and 81.4° corresponding to the (111), (200), (220), (311), and (222) planes, respectively, representing a face-centered cubic (fcc) crystal structure of metallic gold according to the reference (JCPDS file no. 04-0784).[63,64]

The TEM micrograph shown in Figure 5A reveals that the particles are primarily spherical in geometry and are dispersed in two families, around 12.5 and 22.5 nm (Figure 5B). The statistical average size obtained with 500 particles is 19.7 nm. The HRTEM image of a single nanoparticle is shown in Figure 5C, and its corresponding FFT plot is shown in Figure 5D. By applying inverse FFT to the filtered image of Figure 5D with the DigitalMicrograph software, it is possible to reconstruct the crystal structure as shown in Figure 5E. The obtained distances of 2.4, 2.1, and 1.4 Å correspond to the crystalline planes (111), (200), and (220) of fcc metallic gold.[65]

https://doi.org/10.1021/acsomega.1c01506
ACS Omega 2021, 6, 24338−24350

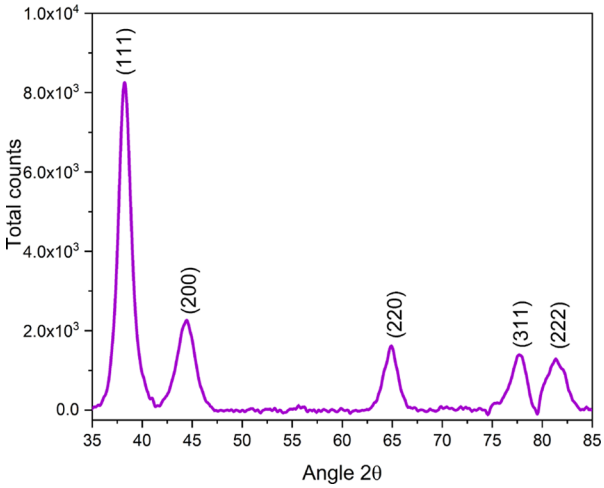

Figure 4. AuVmNPs' XRD pattern.

Figure 6 corresponds to the AuVmNP morphological study using SEM. In Figure 6A, the secondary electron SEM micrograph confirms the nanoparticles' quasi-spherical geometry. Additionally, an enveloping layer around the AuVmNPs is observed. In Figure 6B, the same nanoparticle group was registered in transmission-SEM mode, and in the micrograph, it is no longer possible to distinguish the coverage on the nanoparticles. The obtaining of STEM images with poor contrast for some materials is associated with light elements, suggesting that the extract's molecules form the covering, reinforcing previous spectroscopic technique results. The EDX spectrum of AuVmNPs in Figure 6C indicates that, in addition to gold, only low-atomic-number elements associated with the Vm extract are present in AuVmNPs shown in Figure 6D. Detected copper comes from the TEM grid where the sample was deposited. Also, aluminum corresponds to the support of the SEM equipment where the grid is placed. Interestingly, phosphorus does not appear in the EDX spectrum, indicating that the IP6 compound does not form part of the nanoparticle coverage. CAuNPs were characterized by electronic microscopy. The SEM micrograph in Figure S6A corresponds to nanoparticles characterized by a quasi-spherical geometry. Figure S6B, size distribution obtained from 315 nanoparticles, shows a monomodal distribution with an average statistical size of 13.9 ± 2.7 nm.

Before *in vitro* tests, a study of the stability of AuVmNPs and CAuNPs in phosphate-buffered saline (PBS) and Dulbecco's modified Eagle medium (DMEM) supplemented with 10% FBS was carried out. For this, the behavior of localized surface plasmon resonance (LSPR) of the gold nanoparticles in PBS and DMEM was evaluated by UV−vis spectroscopy when dispersing them at a concentration of 200 μg/mL. This

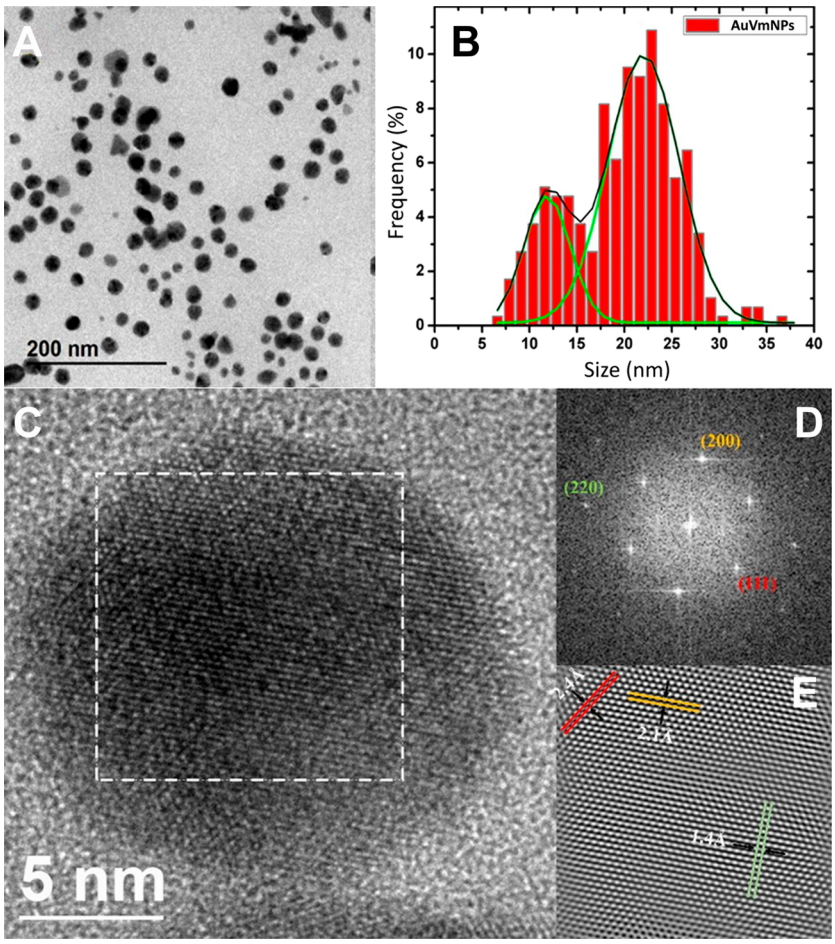

Figure 5. (A) AuVmNPs' TEM micrograph at low magnification. (B) AuVmNPs' size distribution estimated by TEM. (C) AuVmNPs' HRTEM micrograph. (D) Electron diffraction pattern corresponding to the selected square region on (C). The image on (E) corresponds to theoretical reconstruction by inverse FFT from (D). Different crystalline planes can be determined.

https://doi.org/10.1021/acsomega.1c01506
ACS Omega 2021, 6, 24338−24350

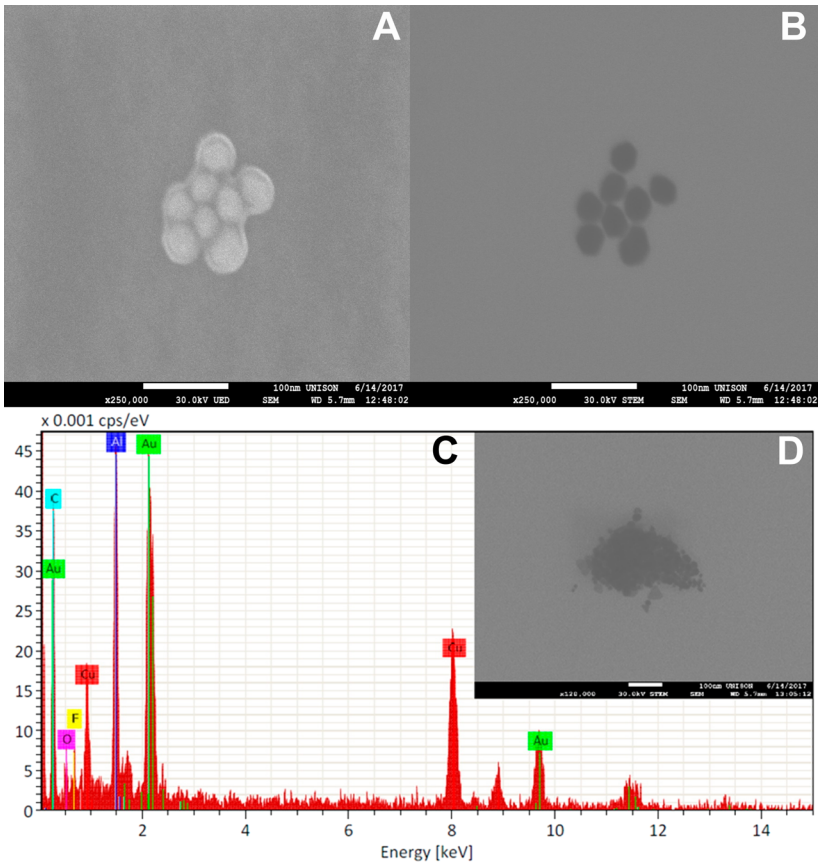

Figure 6. (A) AuVmNPs' SEM micrograph by secondary electrons and (B) micrograph obtained on transmission-SEM mode. (C) AuVmNPs' EDS spectrum corresponding to the nanoparticle group shown in (D).

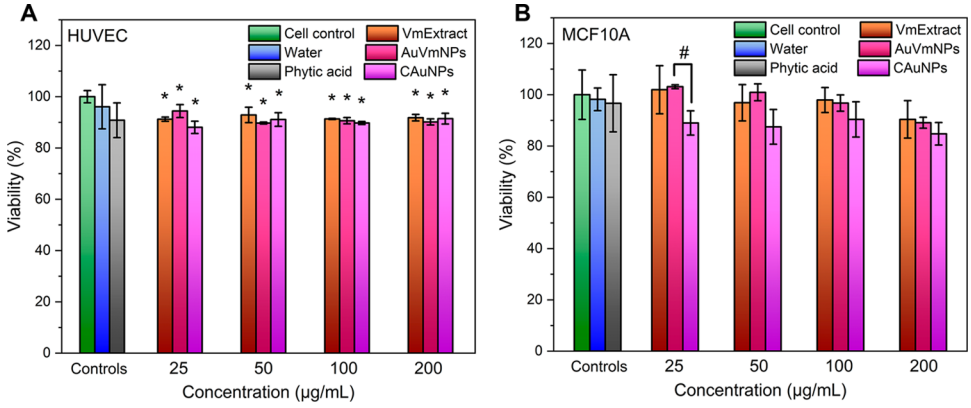

Figure 7. MTT cell viability assay at different concentrations of Vm extract, AuVmNPs, and CAuNPs on (A) HUVECs and (B) MCF10A. One-way ANOVA with the Tukey test. $^{*}p < 0.05$ compared with the cell control, and $^{\#}p < 0.05$ for AuVmNPs vs CAuNPs.

spectroscopic technique allows detecting aggregation processes of nanomaterials or absorption of molecules onto nanoparticle surfaces that give rise to the modification of their absorption spectra.[66,67]

Normalized UV−vis spectra of AuVmNPs and CAuNPs in PBS and water are shown in Figure S7A for comparison. For AuVmNPs, there are no relevant changes in the shape of the spectrum or the position of LSPR (537 nm). On the contrary, for the CAuNP system, the UV−vis spectrum goes from a single well-defined band (523 nm) in water to a spectrum with two bands at 536 and 684 nm in PBS. This suggests that the CAuNP system at a 200 μg/mL concentration in PBS undergoes an aggregation process, forming larger nanostructures. Figure S7B corresponds to the normalized UV−vis spectra of AuVmNPs and CAuNPs in DMEM supplemented with 10% FBS. The UV−vis spectrum does not undergo any modification when dispersing the AuVMNPs in DMEM compared to the signal in water. Interestingly for CAuNPs, the LSPR is located in the same position (523 nm) for both water and DMEM; however, a new band emerges at 582 nm when the system is dispersed in a culture medium. The better stability of the AuVmNP system with respect to CAuNPs in high-ionic-strength environments is attributed to the fact that the extract components sterically stabilize the gold nanoparticles synthesized with *Vitex mollis*. In contrast, citrate gold nanoparticles are electrostatically stabilized.[68] Furthermore,

https://doi.org/10.1021/acsomega.1c01506
ACS Omega 2021, 6, 24338−24350

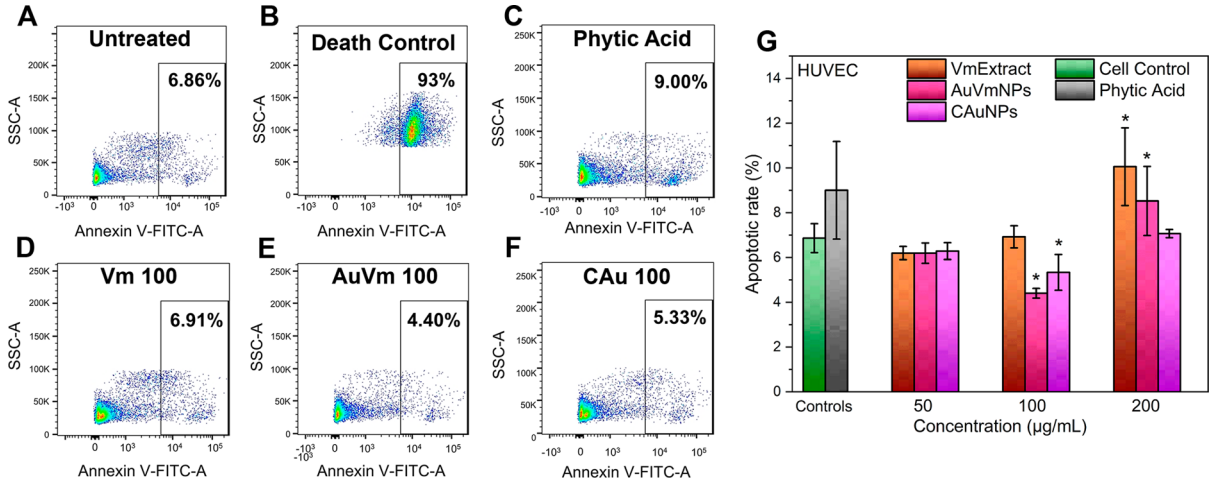

Figure 8. Representative dot plots of apoptotic effects of NPs on HUVECs for (A) untreated control, (B) 70 °C treated as an apoptotic control, (C) phytic acid, (D) *Vitex mollis* extract (100 μg/mL), (E) AuVmNPs (100 μg/mL), and (F) CAuNPs (100 μg/mL). (G) Apoptotic rates of HUVECs with different treatments and concentrations for 24 h determined by annexin V assay using a flow cytometer. One-way ANOVA with the Tukey test. *$p < 0.05$ compared with the cell control. No significant differences were found between AuVmNPs and CAuNPs.

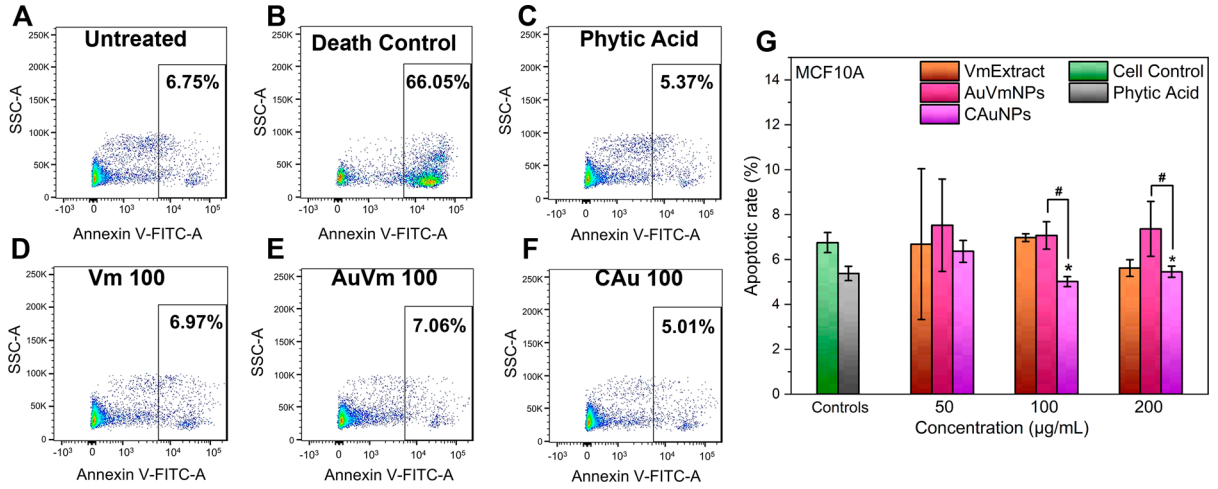

Figure 9. Representative dot plots of apoptotic effects of NPs in MCF10A cells for (A) untreated control, (B) UV light treated as an apoptotic control, (C) phytic acid, (D) *Vitex mollis* extract (100 μg/mL), (E) AuVmNPs (100 μg/mL) and (F) CAuNPs (100 μg/mL). (G) Apoptotic rates of MCF10A cells with different treatments and concentrations for 24 h determined by annexin V assay using a flow cytometer. One-way ANOVA with the Tukey test. *$p < 0.05$ compared with the cell control, and $^{\#}p < 0.05$ for AuVmNPs vs CAuNPs.

there are no indications of protein corona formation for the AuVMNP system in the presence of DMEM supplemented with 10% FBS, indicating a low affinity of the stabilizing compounds adsorbed on the nanoparticles with bovine serum albumin.

The cell viability assay in HUVECs was carried out in the first instance for control agents. Figure 7A shows that ultrapure water, used as a vehicle for CAuNPs, AuVmNPs, IP6, and extract, does not compromise HUVEC viability. Inositol hexakisphosphate (IP6 or phytic acid) concentrations are 12 and 200 μg/mL for the highest concentration of Vm extract. The concentrations evaluated for the AuVmNPs turned out to be nontoxic for the viability assay carried out, obtaining a lower viability percentage for 200 μg/mL concentration with 90.6%, which suggests that AuVmNPs are safe to use. ANOVA with the Tukey test shows significant differences marked with an asterisk (*) with respect to the cell control for $p < 0.05$. Nonsignificant differences were found between AuVmNPs and CAuNPs.

Figure 7B corresponds to the MTT viability assay of the MCF10A cell line treated with AuVmNPs. At the maximum concentration evaluated (200 μg/mL), the viability is 88.7%, suggesting that the AuVmNP system is safe for use in these cells. ANOVA with the Tukey test shows nonsignificative differences of evaluated agents regarding the cell control for $p < 0.05$. Significant differences between AuVmNPs and CAuNPs for 25 μg/mL are marked with #.

Annexin V was used to measure the apoptotic effects of AuVmNPs and CAuNPs on HUVEC and MCF10A cell lines by flow cytometry. Figure 8 corresponds to apoptotic assay in HUVECs. Dot plots of controls indicate that most of the cells are viable (93.14%) in the untreated control (Figure 8A), and phytic acid at 12 μg/mL increases apoptosis by only 2.14% with respect to the untreated control (Figure 8C). From Figure 8D to Figure 8F, representative dot plots for Vm extract, AuVmNPs, and CAuNPs, at 100 μg/mL, show that agents do not induce apoptosis for this concentration. In Figure 8G, it can be appreciated that Vm extract and AuVmNPs at 200 μg/

https://doi.org/10.1021/acsomega.1c01506
ACS Omega 2021, 6, 24338−24350

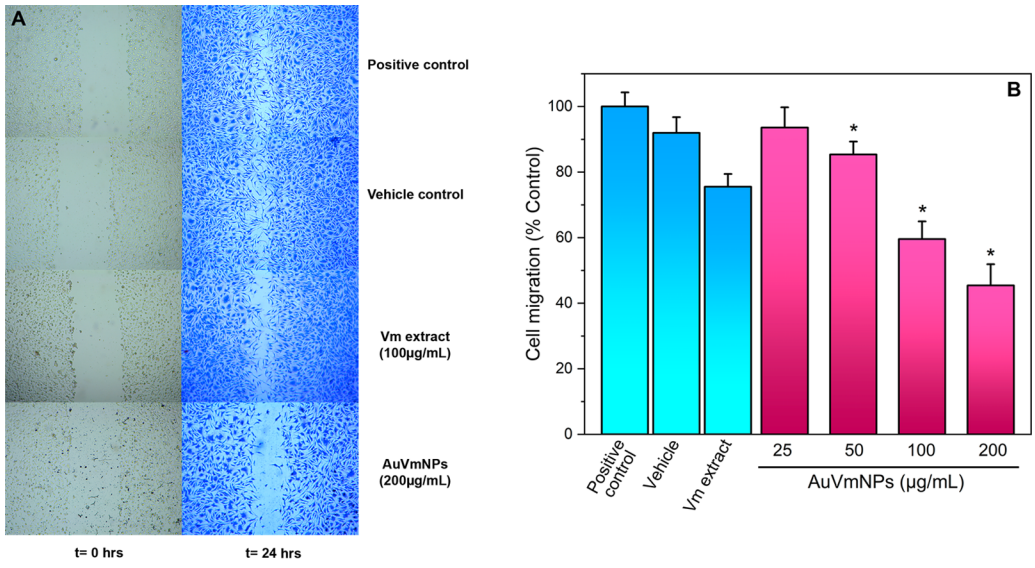

Figure 10. (A) Representative scratch assay of HUVEC cells treated with *Vitex mollis* extract (100 μg/mL) and AuVmNPs (200 μg/mL). (B) Results of mobility inhibition of HUVEC cells treated with AuVmNPs at different concentrations. One-way ANOVA with the Tukey test. *$p < 0.05$ compared with the positive control.

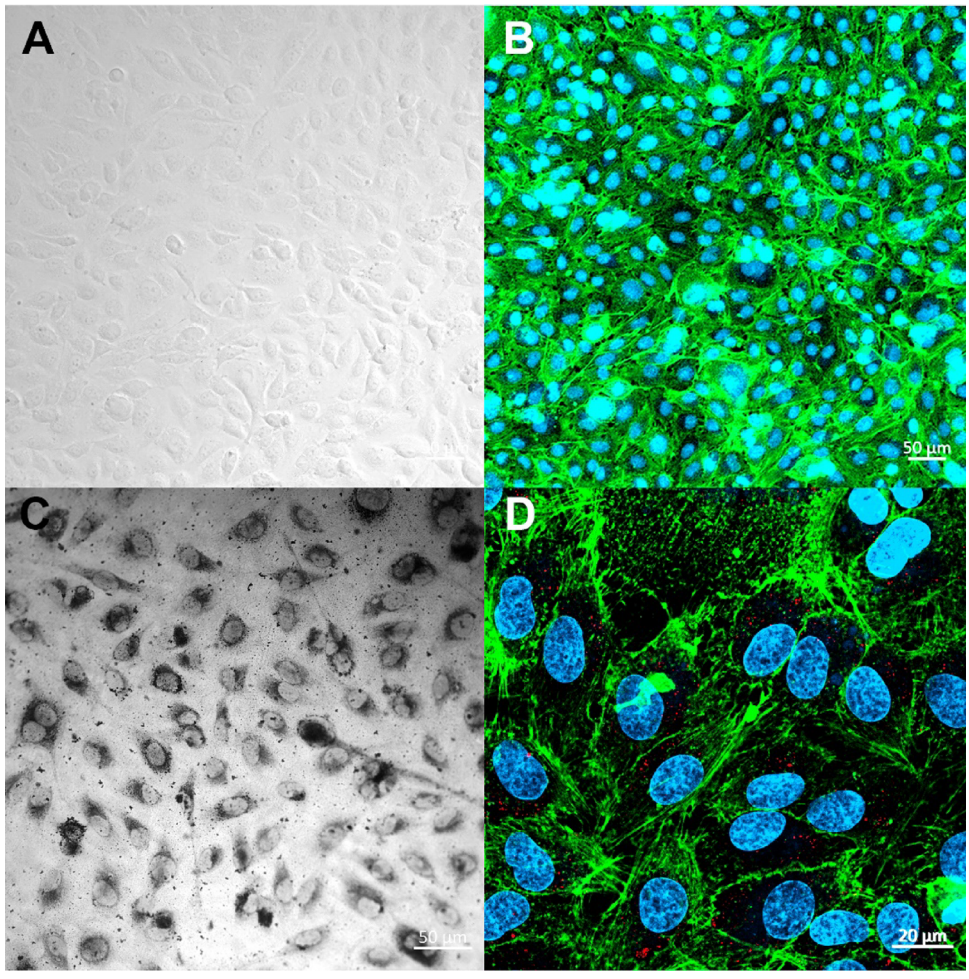

Figure 11. (A) Bright-field image of HUVEC cells without treatment and (B) confocal image where emission from nuclei is shown in blue and actin fibers in green. (C) Bright-field image of HUVEC cells treated with AuVmNPs (50 μg/mL) at 24 h and (D) confocal image where the AuVmNPs are observed in red.

mL increase apoptosis regarding the untreated cell control. This increase is only 1.66% for AuVmNPs and 3.19% for Vm extract, and apoptosis rates do not exceed 10%. There are no significant differences between AuVmNPs and CAuNPs.

https://doi.org/10.1021/acsomega.1c01506
ACS Omega 2021, 6, 24338−24350

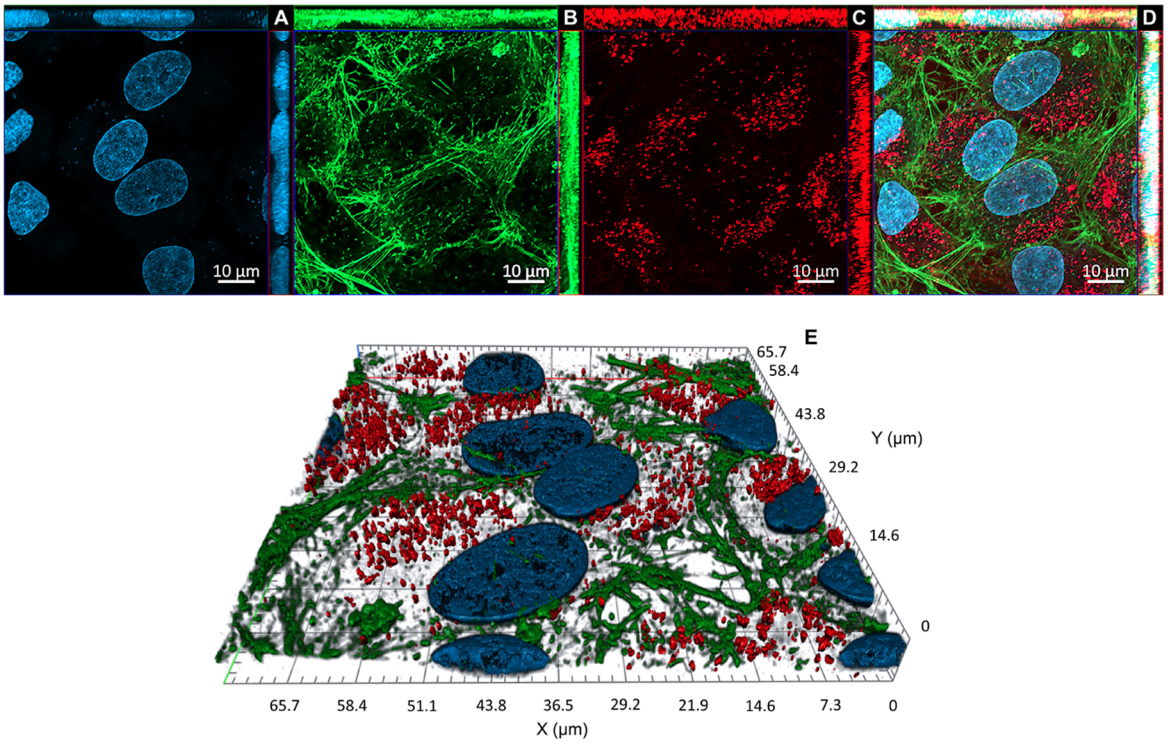

Figure 12. (A–D) Orthogonal projections and (E) 3D image reconstruction of AuVmNP cellular internalization in HUVECs by confocal microscopy.

Results of the apoptotic assay in MCF10A are shown in Figure 9. Interestingly, it is observed that no treatment promotes an increase in apoptosis compared to the control, remaining below 8% in all cases. At 100 and 200 μg/mL, significant differences were found between AuVmNPs and CAuNPs, with apoptosis being slightly lower for the latter. No treatment showed substantial differences regarding the control.

Figure 10 corresponds to cell mobility results. As was done in the viability test, controls and AuVmNPs are tested at different concentrations. In Figure 10A first line, the positive control shows an almost total repopulation in scratch. The second line corresponds to ultrapure water, and the third line is for the extract at a concentration of 100 μg/mL, where a small effect on the cells' mobility is appreciated. The last line of Figure 10 corresponds to AuVmNPs at a 200 μg/mL concentration, showing a significant effect on cell mobility, maintaining a large clear area in the scratch. In Figure 10B, we show the mobility of the HUVECs according to the different concentrations of AuVmNPs, observing a dose-dependent relationship, where the higher the concentration of the NPs, the lower the mobility of the cells. Comparing with the viability results, it can be concluded that the effect on mobility is not due to a toxic effect by the AuVmNPs.[69]

Mukherjee et al. evaluated gold nanoparticle effects on endothelial cells, observing both proliferation and cellular migration.[70] The NPs synthesized in their work by chemical synthesis had a size of 5 nm, the AuNP concentration used was 670 nM, which is equivalent to 514 μg/mL. They observed that nanoparticles are not toxic even at high concentrations. The migration assays obtained an inhibition effect of 80% with the above mentioned concentration. Compared with the AuVmNPs' highest concentration in this work (200 μg/mL), we obtained an inhibition percentage of 55%. However, if we calculate the inhibition/concentration ratio, then we obtain that AuVmNPs present a more significant inhibitory activity in the HUVEC cell migration than that reported by Mukherjee et al. (0.275 versus 0.155 percentage points by μg/mL). On the other hand, Roh and his group demonstrated that gold nanoparticles could induce reorganization in the vascular endothelial cell of growth factor receptor 2 (VEGFR2), which leads to angiogenesis.[65] During angiogenesis, phosphorylation of extracellular regulatory-signaling kinase (ERK), protein kinase B (Akt), and focal adhesion kinase (FAK) triggers proliferation, survival, and migration in cells, respectively, for which Roh et al. observed how AuNPs inhibit phosphorylation of these proteins. This mechanism may explain the AuVmNP inhibitory activity on HUVEC cell migration.

Figure 11A corresponds to the bright-field micrograph of HUVEC cells without AuVmNPs. The same region is shown in the confocal micrograph of Figure 11B, where the cell nuclei (blue) and the actin structures (green) that delimit the cell membranes can be observed. Figure 11C corresponds to a bright-field micrograph of HUVEC cells with AuVmNPs (50 μg/mL). It is observed that the added AuVMNPs have darkened the cells; however, they maintain their stretched shape without appreciable morphological changes that indicate cell death. Figure 11D corresponds to a confocal micrograph of the cells with AuVmNPs. The gold nanoparticles are shown in red; however, the content of these particles is low. This poor content is because the confocal image corresponds only to a reduced focal plane in the *Z*-axis, so only the nanoparticles present in that plane are captured. The AuVmNP distribution study in HUVEC cells was carried out by confocal microscopy through three-dimensional reconstruction. For this, a representative region of 72.44 μm × 72.44 μm × 6.6 μm was selected, and 20 slices of 0.33 μm each were used in the *Z*-stack mode to integrate the 3D image.

https://doi.org/10.1021/acsomega.1c01506
ACS Omega 2021, 6, 24338−24350

Figure 12A−D corresponds to the total projection in the *X*−*Y* plane of the 20 captured cuts and the orthogonal projections. In Figure 12A, we observe the HUVEC cells' nuclei, and Figure 12B corresponds to the actin structures present in the membrane. Figure 12C shows a large abundance of AuVmNPs, and the orthogonal projections in this figure indicate that the particles are uniformly distributed along the *Z*-axis. Similar results are reported by Kotcherlakota et al. in cellular internalization studies by confocal microscopy of gold nanoparticles synthesized with *Zinnia elegans* plant extract, suggesting that the biosynthesized AuNPs facilitate the penetration into the cellular structures.[71] Figure 12D shows the merging of the previous images. AuVmNPs are internalized in the cells but not in the nuclei and distributed throughout the cytosol without a preferential region. This nanoparticle distribution is most clearly illustrated in the three-dimensional reconstruction of Figure 12E.

CONCLUSIONS

The extract obtained from *Vitex mollis* fruit turned out to be a reducing agent appropriate for the synthesis of AuVmNPs through a process framed in the context of green chemistry, which is carried out at room temperature without a greater energy contribution than solar lighting. The UV−vis and FTIR spectra of the AuVmNPs subjected to the cleaning protocol, as well as the scanning electron microscopy images, indicate that compounds from the extract remain adhered to the surface of the NPs, favoring the stability of the systems, which present a net zeta potential greater than −30 mV and an average size of 19.7 ± 5.7 nm.

Viability tests in HUVEC and MCF10A cell lines showed that AuVmNPs are not toxic up to a concentration of 200 μg/mL and do not generate apoptosis at 24 h after exposure to treatment. The scratch assays showed that AuVmNPs have a considerable inhibitory effect on HUVEC cell migration in a dose-dependent form without affecting their viability. The evaluation of the localization of AuVmNPs in HUVECs indicates that nanoparticles penetrate cells and are found in the cytosol without preferential distribution and without entering the nucleus. The low toxicity and the significant inhibitory effect on HUVEC cell migration make AuVmNPs attractive candidates for evaluating suppression of angiogenesis in future studies.

ASSOCIATED CONTENT

Supporting Information

The Supporting Information is available free of charge at https://pubs.acs.org/doi/10.1021/acsomega.1c01506.

(Figure S1) Representative dot plots from (A) all the HUVECs collected, (B,C) selected from region 1 (R1) with whole and structured HUVEC cells (R2 and R3), and (D) annexin V binding analysis coming from R3 cells; (Figure S2) behavior associated with polymers (melanins) consisting of a linear response with a negative slope (for VM extract, the slope has a value of −0.0046 nm^{-1}); (Figure S3) UV−vis spectra for synthesized AuVmNPs captured at various times while the reaction was carried out for 100 min; (Figure S4) UV−vis spectrum for CAuNPs with a maximum at 526 nm; (Figure S5) CAuNPs' (A) zeta potential and (B) DLS; (Figure S6) CAuNPs by (A) SEM and (B) size distribution; (Figure S7) normalized UV−vis spectra of AuVmNPs and CAuNPs in (A) PBS and (B) DMEM supplemented with 10% FBS (obtained spectra at a gold nanoparticle concentration of 200 μg/mL) (PDF)

AUTHOR INFORMATION

Corresponding Author

Ramón Iñiguez-Palomares − *Nanotechnology Graduate Program, Department of Physics, Universidad de Sonora, Hermosillo, Sonora 83000, Mexico;* orcid.org/0000-0002-9218-936X; Email: ramon.iniguez@unison.mx

Authors

Abraham Arizmendi-Grijalva − *Nanotechnology Graduate Program, Department of Physics, Universidad de Sonora, Hermosillo, Sonora 83000, Mexico*

Aarón Alberto Martínez-Higuera − *Nanotechnology Graduate Program, Department of Physics, Universidad de Sonora, Hermosillo, Sonora 83000, Mexico*

Jesús Adriana Soto-Guzmán − *Department of Medicine and Health Science, Universidad de Sonora, Hermosillo, Sonora 83000, Mexico*

Juan Manuel Martínez-Soto − *Department of Medicine and Health Science, Universidad de Sonora, Hermosillo, Sonora 83000, Mexico*

Ericka Rodríguez-León − *Nanotechnology Graduate Program, Department of Physics, Universidad de Sonora, Hermosillo, Sonora 83000, Mexico;* orcid.org/0000-0002-5928-8796

César Rodríguez-Beas − *Nanotechnology Graduate Program, Department of Physics, Universidad de Sonora, Hermosillo, Sonora 83000, Mexico*

Luis Fernando López-Soto − *Department of Medicine and Health Science, Universidad de Sonora, Hermosillo, Sonora 83000, Mexico*

Francisco Javier Alvarez-Cirerol − *Health Sciences Graduate Program, Department of Biological Chemistry, Universidad de Sonora, Hermosillo, Sonora 83000, Mexico*

Nadia Garcia-Flores − *Nanotechnology Graduate Program, Department of Physics, Universidad de Sonora, Hermosillo, Sonora 83000, Mexico*

Pedro Cortés-Reynosa − *Departamento de Biología Celular, Cinvestav-IPN, 07360 Mexico DF, Mexico*

Eduardo Pérez-Salazar − *Departamento de Biología Celular, Cinvestav-IPN, 07360 Mexico DF, Mexico*

Complete contact information is available at: https://pubs.acs.org/10.1021/acsomega.1c01506

Notes

The authors declare no competing financial interest.

ACKNOWLEDGMENTS

TEM analysis was supported by the Scanning Electron Microscopy Lab of the Physics Department. All authors want to acknowledge the Biomaterials Laboratory for the use of a confocal microscope of the Physics Department, University of Sonora. A.A.-G. would like to thank Conacyt for Doctoral Fellowship number 748633, and A.A.M.-H. would like to thank Conacyt for Post-Doctoral Fellowship (2019-000019-01NACV-00449), support number 740180.

REFERENCES

(1) Abdalla, S. S. I.; Katas, H.; Azmi, F.; Busra, M. F. M. Antibacterial and Anti-Biofilm Biosynthesised Silver and Gold Nanoparticles for Medical Applications: Mechanism of Action, Toxicity and Current Status. *Curr. Drug Delivery* **2020**, *17*, 88−100.

(2) Tan, G.; Onur, M. A. Cellular Localization and Biological Effects of 20nm-Gold Nanoparticles. *J. Biomed. Mater. Res. A* **2018**, *106*, 1708−1721.

(3) Apaolaza, P. S.; Busch, M.; Asin-Prieto, E.; Peynshaert, K.; Rathod, R.; Remaut, K.; Dünker, N.; Göpferich, A. Hyaluronic Acid Coating of Gold Nanoparticles for Intraocular Drug Delivery: Evaluation of the Surface Properties and Effect on Their Distribution. *Exp. Eye Res.* **2020**, *198*, 108151.

(4) Singh, R.; Batoki, J. C.; Ali, M.; Bonilha, V. L.; Anand-Apte, B. Inhibition of Choroidal Neovascularization by Systemic Delivery of Gold Nanoparticles. *Nanomedicine* **2020**, *28*, 102205.

(5) Arib, C.; Spadavecchia, J. Lenalidomide (LENA) Hybrid Gold Complex Nanoparticles: Synthesis, Physicochemical Evaluation, and Perspectives in Nanomedicine. *ACS Omega* **2020**, *5*, 28483−28492.

(6) Saeed, B. A.; Lim, V.; Yusof, N. A.; Khor, K. Z.; Rahman, H. S.; Samad, N. A. Antiangiogenic Properties of Nanoparticles: A Systematic Review. *Int. J. Nanomed.* **2019**, *Volume 14*, 5135−5146.

(7) Kajani, A. A.; Bordbar, A.-K.; Zarkesh Esfahani, S. H.; Razmjou, A. Gold Nanoparticles as Potent Anticancer Agent: Green Synthesis, Characterization, and in Vitro Study. *RSC Adv.* **2016**, *6*, 63973−63983.

(8) Farooq, M. U.; Novosad, V.; Rozhkova, E. A.; Wali, H.; Ali, A.; Fateh, A. A.; Neogi, P. B.; Neogi, A.; Wang, Z. Gold Nanoparticles-Enabled Efficient Dual Delivery of Anticancer Therapeutics to HeLa Cells. *Sci. Rep.* **2018**, *8*, 2907.

(9) Alsammarraie, F. K.; Wang, W.; Zhou, P.; Mustapha, A.; Lin, M. Green Synthesis of Silver Nanoparticles Using Turmeric Extracts and Investigation of Their Antibacterial Activities. *Colloids Surf., B* **2018**, *171*, 398−405.

(10) Yadi, M.; Mostafavi, E.; Saleh, B.; Davaran, S.; Aliyeva, I.; Khalilov, R.; Nikzamir, M.; Nikzamir, N.; Akbarzadeh, A.; Panahi, Y.; Milani, M. Current Developments in Green Synthesis of Metallic Nanoparticles Using Plant Extracts: A Review. *Artif. Cells Nanomed., Biotechnol.* **2018**, *46*, S336−S343.

(11) Khan, Z. U. H.; Khan, A.; Chen, Y.; Shah, N. S.; Muhammad, N.; Khan, A. U.; Tahir, K.; Khan, F. U.; Murtaza, B.; Hassan, S. U.; Qaisrani, S. A.; Wan, P. Biomedical Applications of Green Synthesized Nobel Metal Nanoparticles. *J. Photochem. Photobiol.: B* **2017**, *173*, 150−164.

(12) Md Ishak, N. A. I.; Kamarudin, S. K.; Timmiati, S. N. Green Synthesis of Metal and Metal Oxide Nanoparticles via Plant Extracts: An Overview. *Mater. Res. Express* **2019**, *6*, 112004.

(13) Rana, A.; Yadav, K.; Jagadevan, S. A Comprehensive Review on Green Synthesis of Nature-Inspired Metal Nanoparticles: Mechanism, Application and Toxicity. *J. Clean. Prod.* **2020**, *272*, 122880.

(14) *Metal Nanoparticles for Drug Delivery and Diagnostic Applications*; Elsevier: 2020.

(15) Nirmala, J. G.; Akila, S.; Nadar, M. S. A. M.; Narendhirakannan, R. T.; Chatterjee, S. Biosynthesized *Vitis Vinifera* Seed Gold Nanoparticles Induce Apoptotic Cell Death in A431 Skin Cancer Cells. *RSC Adv.* **2016**, *6*, 82205−82218.

(16) Stankus, D. P.; Lohse, S. E.; Hutchison, J. E.; Nason, J. A. Interactions between Natural Organic Matter and Gold Nanoparticles Stabilized with Different Organic Capping Agents. *Environ. Sci. Technol.* **2011**, *45*, 3238−3244.

(17) Arasu, M. V.; Arokiyaraj, S.; Viayaraghavan, P.; Kumar, T. S. J.; Duraipandiyan, V.; Al-Dhabi, N. A.; Kaviyarasu, K. One Step Green Synthesis of Larvicidal, and Azo Dye Degrading Antibacterial Nanoparticles by Response Surface Methodology. *J. Photochem. Photobiol.: B* **2019**, *190*, 154−162.

(18) Hanahan, D.; Weinberg, R. A. Hallmarks of Cancer: The next Generation. *Cell* **2011**, *144*, 646−674.

(19) *Biology of Endothelial Cells*; Jaffe, E. A. Ed.; Developments in Cardiovascular Medicine; Kluwer Academic: Tucson, AZ, 1984.

(20) Nishida, N.; Yano, H.; Nishida, T.; Kamura, T.; Kojiro, M. Angiogenesis in Cancer. *Vasc. Health Risk Manag.* **2006**, *2*, 213−219.

(21) Vimalraj, S.; Ashokkumar, T.; Saravanan, S. Biogenic Gold Nanoparticles Synthesis Mediated by *Mangifera Indica* Seed Aqueous Extracts Exhibits Antibacterial, Anticancer and Anti-Angiogenic Properties. *Biomed. Pharmacother.* **2018**, *105*, 440−448.

(22) Arvizo, R. R.; Rana, S.; Miranda, O. R.; Bhattacharya, R.; Rotello, V. M.; Mukherjee, P. Mechanism of Anti-Angiogenic Property of Gold Nanoparticles: Role of Nanoparticle Size and Surface Charge. *Nanomedicine* **2011**, *7*, 580−587.

(23) Roma-Rodrigues, C.; Fernandes, A. R.; Baptista, P. V. Counteracting the Effect of Leukemia Exosomes by Antiangiogenic Gold Nanoparticles. *Int. J. Nanomed.* **2019**, *Volume 14*, 6843−6854.

(24) Al-Trad, B.; Aljabali, A.; Al Zoubi, M.; Shehab, M.; Omari, S. Effect of Gold Nanoparticles Treatment on the Testosterone-Induced Benign Prostatic Hyperplasia in Rats. *Int. J. Nanomed.* **2019**, *Volume 14*, 3145−3154.

(25) Darweesh, R. S.; Ayoub, N. M.; Nazzal, S. Gold Nanoparticles and Angiogenesis: Molecular Mechanisms and Biomedical Applications. *Int. J. Nanomed.* **2019**, *Volume 14*, 7643−7663.

(26) Sanfilippo, V.; Caruso, V. C. L.; Cucci, L. M.; Inturri, R.; Vaccaro, S.; Satriano, C. Hyaluronan-Metal Gold Nanoparticle Hybrids for Targeted Tumor Cell Therapy. *Int. J. Mol. Sci.* **2020**, *21*, 3085.

(27) Rajora, A. K.; Ravishankar, D.; Zhang, H.; Rosenholm, J. M. Recent Advances and Impact of Chemotherapeutic and Antiangiogenic Nanoformulations for Combination Cancer Therapy. *Pharmaceutics* **2020**, *12*, 592.

(28) Chan, C.-M.; Hsiao, C.-Y.; Li, H.-J.; Fang, J.-Y.; Chang, D.-C.; Hung, C.-F. The Inhibitory Effects of Gold Nanoparticles on VEGF-A-Induced Cell Migration in Choroid-Retina Endothelial Cells. *Int. J. Mol. Sci.* **2020**, *21*, 109.

(29) Pan, Y.; Wu, Q.; Qin, L.; Cai, J.; Du, B. Gold Nanoparticles Inhibit $VEGF_{165}$-Induced Migration and Tube Formation of Endothelial Cells via the Akt Pathway. *Biomed. Res. Int.* **2014**, *2014*, 418624.

(30) Nethi, S. K.; Mukherjee, S.; Veeriah, V.; Barui, A. K.; Chatterjee, S.; Patra, C. R. Bioconjugated Gold Nanoparticles Accelerate the Growth of New Blood Vessels through Redox Signaling. *Chem. Commun.* **2014**, *50*, 14367−14370.

(31) Montiel-Herrera, M.; Camacho-Hernández, I. L.; Ríos-Morgan, A.; Delgado-Vargas, F. Partial Physicochemical and Nutritional Characterization of the Fruit of *Vitex Mollis* (Verbenaceae). *J. Food Compost. Anal.* **2004**, *17*, 205−215.

(32) Apte, M.; Girme, G.; Nair, R.; Bankar, A.; Ravi Kumar, A.; Zinjarde, S. Melanin Mediated Synthesis of Gold Nanoparticles by Yarrowia Lipolytica. *Mater. Lett.* **2013**, *95*, 149−152.

(33) Pralea, I.-E.; Moldovan, R.-C.; Petrache, A.-M.; Ilieş, M.; Hegheş, S.-C.; Ielciu, I.; Nicoară, R.; Moldovan, M.; Ene, M.; Radu, M.; Uifălean, A.; Iuga, C.-A. From Extraction to Advanced Analytical Methods: The Challenges of Melanin Analysis. *Int. J. Mol. Sci.* **2019**, *20*, 3943.

(34) Roy, S.; Shankar, S.; Rhim, J.-W. Melanin-Mediated Synthesis of Silver Nanoparticle and Its Use for the Preparation of Carrageenan-Based Antibacterial Films. *Food Hydrocolloids* **2019**, *88*, 237−246.

(35) Kiran, G. S.; Dhasayan, A.; Lipton, A. N.; Selvin, J.; Arasu, M. V.; Al-Dhabi, N. A. Melanin-Templated Rapid Synthesis of Silver Nanostructures. *J. Nanobiotechnol.* **2014**, *12*, 18.

(36) Dong, H.; Liu, Z.; Zhong, H.; Yang, H.; Zhou, Y.; Hou, Y.; Long, J.; Lin, J.; Guo, Z. Melanin-Associated Synthesis of SERS-Active Nanostructures and the Application for Monitoring of Intracellular Melanogenesis. *Nanomaterials* **2017**, *7*, 70.

(37) Gurme, S. T.; Aware, C. B.; Surwase, S. N.; Chavan, C. S.; Jadhav, J. P. Synthesis of Melanin Mediated Silver Nanoparticles from *Aeromonas* Sp. SNS Using Response Surface Methodology: Characterization with the Biomedical Applications and Photocatalytic Degradation of Brilliant Green. *J. Polym. Environ.* **2019**, *27*, 2428−2438.

https://doi.org/10.1021/acsomega.1c01506
ACS Omega 2021, 6, 24338−24350

(38) Dobrowolska, P.; Krajewska, A.; Gajda-Rączka, M.; Bartosewicz, B.; Nyga, P.; Jankiewicz, B. Application of Turkevich Method for Gold Nanoparticles Synthesis to Fabrication of SiO_2@Au and TiO_2@Au Core-Shell Nanostructures. *Materials* **2015**, *8*, 2849−2862.
(39) Jiménez-Estrada, M.; Velázquez-Contreras, C.; Garibay-Escobar, A.; Sierras-Canchola, D.; Lapizco-Vázquez, R.; Ortiz-Sandoval, C.; Burgos-Hernández, A.; Robles-Zepeda, R. E. *In Vitro* Antioxidant and Antiproliferative Activities of Plants of the Ethnopharmacopeia from Northwest of Mexico. *BMC Complement. Altern. Med.* **2013**, *13*, 12.
(40) Cuevas-Juárez, E.; Yuriar-Arredondo, K. Y.; Pío-León, J. F.; Montes-Avila, J.; López-Angulo, G.; Páz Díaz-Camacho, S.; Delgado-Vargas, F. Antioxidant and α-Glucosidase Inhibitory Properties of Soluble Melanins from the Fruits of *Vitex Mollis* Kunth, *Randia Echinocarpa* Sessé et Mociño and *Crescentia Alata* Kunth. *J. Funct. Foods* **2014**, *9*, 78−88.
(41) Rajagopal, K.; Kathiravan, G.; Karthikeyan, S. Extraction and Characterization of Melanin from Phomopsis: A Phellophytic Fungi Isolated from Azadirachta Indica A. Juss. *Afr. J. Microbiol. Res.* **2011**, *5*, 762−766.
(42) Sava, V. M.; Yang, S.-M.; Hong, M.-Y.; Yang, P.-C.; Huang, G. S. Isolation and Characterization of Melanic Pigments Derived from Tea and Tea Polyphenols. *Food Chem.* **2001**, *73*, 177−184.
(43) Pío-León, J. F.; Montes-Avila, J.; López-Angulo, G.; Díaz-Camacho, S. P.; Vega-Rios, A.; López-Valenzuela, J. Á.; Delgado-Vargas, F. Melanins Of *Vitex Mollis* fruit with Differences in Water-Solubility Show High Inhibition of Carbohydrate Digestive Enzymes and Antioxidant Activity. *J. Food Biochem.* **2018**, *42*, No. e12509.
(44) Ou-Yang, H.; Stamatas, G.; Kollias, N. Spectral Responses of Melanin to Ultraviolet A Irradiation. *J. Invest. Dermatol.* **2004**, *122*, 492−496.
(45) Kim, D. J.; Ju, K.-Y.; Lee, J.-K. The Synthetic Melanin Nanoparticles Having an Excellent Binding Capacity of Heavy Metal Ions. *Bull. Korean Chem. Soc.* **2012**, *33*, 3788−3792.
(46) Yao, Z.; Qi, J.; Wang, L. Isolation, Fractionation and Characterization of Melanin-like Pigments from Chestnut (*Castanea Mollissima*) Shells. *J. Food Sci.* **2012**, *77*, C671−C676.
(47) Hussain, M. H.; Abu Bakar, N. F.; Mustapa, A. N.; Low, K.-F.; Othman, N. H.; Adam, F. Synthesis of Various Size Gold Nanoparticles by Chemical Reduction Method with Different Solvent Polarity. *Nanoscale Res. Lett.* **2020**, *15*, 140.
(48) Kumar, V.; Yadav, S. K. Characterisation of Gold Nanoparticles Synthesised by Leaf and Seed Extract Of *Syzygium Cumini* L. *J. Exp. Nanosci.* **2012**, *7*, 440−451.
(49) Megarajan, S.; Ahmed, K. B. A.; Reddy, G. R. K.; Kumar, P. S.; Anbazhagan, V. Phytoproteins in Green Leaves as Building Blocks for Photosynthesis of Gold Nanoparticles: An Efficient Electrocatalyst towards the Oxidation of Ascorbic Acid and the Reduction of Hydrogen Peroxide. *J. Photochem. Photobiol.: B* **2016**, *155*, 7−12.
(50) Vo, T.-T.; Nguyen, T. T.-N.; Huynh, T. T.-T.; Vo, T. T.-T.; Nguyen, T. T.-N.; Nguyen, D.-T.; Dang, V.-S.; Dang, C.-H.; Nguyen, T.-D. Biosynthesis of Silver and Gold Nanoparticles Using Aqueous Extract from *Crinum Latifolium* Leaf and Their Applications Forward Antibacterial Effect and Wastewater Treatment. *J. Nanomater.* **2019**, *2019*, 1−14.
(51) Montes-Avila, J.; Ojeda-Ayala, M.; López-Angulo, G.; Pío-León, J. F.; Díaz-Camacho, S. P.; Ochoa-Terán, A.; Delgado-Vargas, F. Physicochemical Properties and Biological Activities of Melanins from the Black-Edible Fruits *Vitex Mollis* and *Randia Echinocarpa*. *J. Food Meas. Charact.* **2018**, *12*, 1972−1980.
(52) Shoeva, O. Y.; Mursalimov, S. R.; Gracheva, N. V.; Glagoleva, A. Y.; Börner, A.; Khlestkina, E. K. Melanin Formation in Barley Grain Occurs within Plastids of Pericarp and Husk Cells. *Sci. Rep.* **2020**, *10*, 179.
(53) Glagoleva, A. Y.; Shoeva, O. Y.; Khlestkina, E. K. Melanin Pigment in Plants: Current Knowledge and Future Perspectives. *Front. Plant Sci.* **2020**, *11*, 770.
(54) Solano, F. Melanins: Skin Pigments and Much More—Types, Structural Models, Biological Functions, and Formation Routes. *New J. Sci.* **2014**, *2014*, 1−28.
(55) Gebru, H.; Cui, S.; Li, Z.; Wang, X.; Pan, X.; Liu, J.; Guo, K. Facile PH-Dependent Synthesis and Characterization of Catechol Stabilized Silver Nanoparticles for Catalytic Reduction of 4-Nitrophenol. *Catal. Lett.* **2017**, *147*, 2134−2143.
(56) Seo, Y. S.; Ahn, E.-Y.; Park, J.; Kim, T. Y.; Hong, J. E.; Kim, K.; Park, Y.; Park, Y. Catalytic Reduction of 4-Nitrophenol with Gold Nanoparticles Synthesized by Caffeic Acid. *Nanoscale Res. Lett.* **2017**, *12*, 7.
(57) Hwang, S. J.; Jun, S. H.; Park, Y.; Cha, S.-H.; Yoon, M.; Cho, S.; Lee, H.-J.; Park, Y. Green Synthesis of Gold Nanoparticles Using Chlorogenic Acid and Their Enhanced Performance for Inflammation. *Nanomedicine* **2015**, *11*, 1677−1688.
(58) Martínez-Castañón, G. A.; Niño-Martínez, N.; Martínez-Gutierrez, F.; Martínez-Mendoza, J. R.; Ruiz, F. Synthesis and Antibacterial Activity of Silver Nanoparticles with Different Sizes. *J. Nanopart. Res.* **2008**, *10*, 1343−1348.
(59) Halder, A.; Das, S.; Ojha, D.; Chattopadhyay, D.; Mukherjee, A. Highly Monodispersed Gold Nanoparticles Synthesis and Inhibition of Herpes Simplex Virus Infections. *Mater. Sci. Eng.: C* **2018**, *89*, 413−421.
(60) Amini, S. M.; Akbari, A. Metal Nanoparticles Synthesis through Natural Phenolic Acids. *IET Nanobiotechnol.* **2019**, *13*, 771−777.
(61) Guo, D.; Dou, D.; Ge, L.; Huang, Z.; Wang, L.; Gu, N. A Caffeic Acid Mediated Facile Synthesis of Silver Nanoparticles with Powerful Anti-Cancer Activity. *Colloids Surf., B* **2015**, *134*, 229−234.
(62) Mapala, K.; Pattabi, M. *Mimosa Pudica* Flower Extract Mediated Green Synthesis of Gold Nanoparticles. *NanoWorld J.* **2017**, *03*, 44−50.
(63) Umamaheswari, C.; Lakshmanan, A.; Nagarajan, N. S. Green Synthesis, Characterization and Catalytic Degradation Studies of Gold Nanoparticles against Congo Red and Methyl Orange. *J. Photochem. Photobiol.: B* **2018**, *178*, 33−39.
(64) Zha, J.; Dong, C.; Wang, X.; Zhang, X.; Xiao, X.; Yang, X. Green Synthesis and Characterization of Monodisperse Gold Nanoparticles Using Ginkgo Biloba Leaf Extract. *Optik* **2017**, *144*, 511−521.
(65) Roh, Y. J.; Rho, C. R.; Cho, W. K.; Kang, S. The antiangiogenic effects of gold nanoparticles on experimental choroidal neovascularization in mice. *Invest. Ophthalmol. Visual Sci.* **2016**, *57* (15), 6561−6567.
(66) Boldeiu, A.; Simion, M.; Mihalache, I.; Radoi, A.; Banu, M.; Varasteanu, P.; Nadejde, P.; Vasile, E.; Acasandrei, A.; Popescu, R. C.; Savu, D.; Kusko, M. Comparative Analysis of Honey and Citrate Stabilized Gold Nanoparticles: In Vitro Interaction with Proteins and Toxicity Studies. *J. Photochem. Photobiol.: B* **2019**, *197*, 111519.
(67) Barreto, Â.; Luis, L. G.; Girão, A. V.; Trindade, T.; Soares, A. M. V. M.; Oliveira, M. Behavior of Colloidal Gold Nanoparticles in Different Ionic Strength Media. *J. Nanopart. Res.* **2015**, *17*, 493.
(68) Moore, T. L.; Rodriguez-Lorenzo, L.; Hirsch, V.; Balog, S.; Urban, D.; Jud, C.; Rothen-Rutishauser, B.; Lattuada, M.; Petri-Fink, A. Nanoparticle Colloidal Stability in Cell Culture Media and Impact on Cellular Interactions. *Chem. Soc. Rev.* **2015**, *44*, 6287−6305.
(69) Balakrishnan, S.; Bhat, F. A.; Raja Singh, P.; Mukherjee, S.; Elumalai, P.; Das, S.; Patra, C. R.; Arunakaran, J. Gold Nanoparticle-Conjugated Quercetin Inhibits Epithelial-Mesenchymal Transition, Angiogenesis and Invasiveness *via* EGFR/VEGFR-2-Mediated Pathway in Breast Cancer. *Cell Prolif.* **2016**, *49*, 678−697.
(70) Mukherjee, P.; Bhattacharya, R.; Wang, P.; Wang, L.; Basu, S.; Nagy, J. A.; Atala, A.; Mukhopadhyay, D.; Soker, S. Antiangiogenic Properties of Gold Nanoparticles. *Clin. Cancer Res.* **2005**, *11*, 3530−3534.
(71) Kotcherlakota, R.; Nimushakavi, S.; Roy, A.; Yadavalli, H. C.; Mukherjee, S.; Haque, S.; Patra, C. R. Biosynthesized Gold Nanoparticles: *In Vivo* Study of near-Infrared Fluorescence (NIR)-Based Bio-Imaging and Cell Labeling Applications. *ACS Biomater. Sci. Eng.* **2019**, *5*, 5439−5452.

https://doi.org/10.1021/acsomega.1c01506
ACS Omega 2021, 6, 24338−24350